Modeling rf sheath formation in turbulent tokamak boundary plasma

Thomas G. Jenkins[1*], *David N.* Smithe[1], *Maxim V.* Umansky[2], *James R.* Myra[3], and *Benjamin D.* Dudson[2]

[1]Silvaco, Inc., Boulder, Colorado 80303, United States
[2]Lawrence Livermore National Laboratory, Livermore, California 94550, United States
[3]Lodestar Research Corporation, Broomfield, Colorado 80023, United States

Abstract. During ICRF antenna operation, complex interactions between turbulent density profiles, nonlinear RF sheaths, and RF-induced convective transport are observed to alter plasma density in the tokamak edge [D'Ippolito *et al*., Nucl. Fusion **38**, 1543 (1998)]. In this work, we explore the physics of such interactions via numerical modeling, using a nonlinear EM/plasma/sheath code (VSim) and profiles obtained from a fluid plasma turbulence code (Hermes) in a 3D slab domain containing biased side-wall limiters. RF-rectified sheath formation on antenna and limiter surfaces is observed as electromagnetic waves launched by the antenna are refracted through the turbulent density profile. On transport timescales, such sheath potentials have been shown to influence both the mean species density and its RMS fluctuation spectrum [Smithe *et al*., these proceedings]. On the faster RF timescales, we demonstrate that the converse is also true – regions of high plasma density near material surfaces give rise to the highest sheath potential amplitudes. When density is turbulent and spatially nonuniform, localized regions of high sheath potential (hotspots) may develop where high-density filaments intersect material surfaces. Such hotspots are of particular concern as sources of impurity sputtering, and we explore their behavior in response to changes both to the local plasma density and to antenna operating parameters and structure. Related results exploring the role of Faraday shields and/or enclosing structures in suppressing high sheath potentials for other devices (e.g. SPARC) will also be shown.

Complex interactions between turbulent density profiles, nonlinear RF sheath potentials, and RF-induced convective transport are observed to alter plasma density in the tokamak edge during ICRF antenna operation [1]. This work summarizes recent efforts to explore the physics of such interactions using numerical modeling tools. Conceptually similar work, exploring various aspects of the interaction between turbulent density filaments and ICRF fields, has been carried out by other authors using analytic or numerically generated profiles for the filaments [2, 3]. In this work we will primarily focus on the interaction of self-consistent, numerically-generated density filaments with RF-induced sheaths.

The physical domain we will consider in this work is a flux tube in the tokamak edge[†] – a geometry highly elongated along the direction of the magnetic field ('parallel') and comparatively narrow in its perpendicular dimensions. Since we are concerned with the role of ICRF, we will specify that this flux tube is partially intercepted by two limiter plates, and will further assume that an RF antenna is positioned between these plates. In a typical ICRF antenna, antenna straps oriented in the 'binormal' direction (i.e., perpendicular to both the radial and parallel directions) are positioned within an aperture bounded by protective limiter structures, and current driven in these straps excites electromagnetic waves that (ideally) propagate radially inward toward the tokamak core. We will assert that our flux tube of interest consists of a number of parallel field lines which pass just in front of (i.e., radially inward from) such an antenna aperture, as well as their neighboring field lines which intercept the limiter walls surrounding the aperture; roughly half of the perpendicular cross-section of the flux tube will thus be shadowed by the limiter.

Since field-line curvature effects are not critical to the physics we will initially consider, we represent our flux tube of interest as a 3D straight slab, shown schematically in Figure 1L. The slab has characteristic lengths (0.1 m, 20.0 m, 1.0 m) in the (x,y,z) directions; respectively, these coordinates correspond to the radial, parallel, and binormal directions in tokamak edge plasma. Two solid limiter plates span the full domain (from z=0.0 m to z=1.0 m) in the z/binormal coordinate and half of the domain (from x=0.05 m to x=0.1 m) in the x/radial coordinate; in the parallel coordinate they extend from y=6.53 m to y=6.74 m for the bottom limiter and from y=8.21 m to 8.42 m for the top limiter.

* Corresponding author: thomas.jenkins@silvaco.com
[†] Other research published in these conference proceedings also uses this flux-tube model; see D. N. Smithe *et al*., "Modeling of Turbulence, Transport, and RF-induced Convective Cells in Tokamak Boundary Plasma", for additional discussion and motivation.

A static background magnetic field of strength B=0.5 T points in the y/parallel direction.

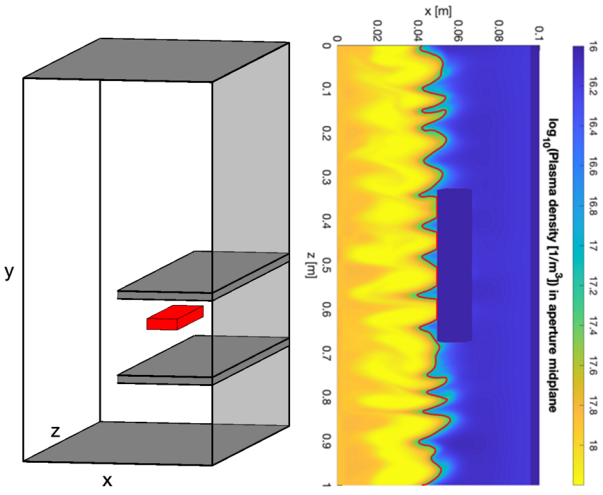

Fig. 1. (Left) Flux-tube geometry used in the Hermes and VSim simulations, shown in the single-strap configuration. Two limiter plates, which shadow half of the cross-sectional area of the flux tube, surround an RF antenna strap. The core plasma is to the left of the diagram (lower x) while the vacuum vessel is schematically represented at the right (upper x face). (Right) Representative turbulent plasma density in the cross-sectional x-z plane midway between the limiter plates, as predicted by Hermes. Significant density reduction is observed within the antenna aperture due to the protective limiters, which extend from x=0.05 to x=0.1. The S = 0 resonant surface (at n_0 = 1.75 x 10^{17} / m^3) is shown in red; positive S values are to the right of this line.

Recent studies [4] using this flux-tube geometry exercised the Hermes code [5, 6] to examine the effect of RF sheath potential formation on the evolution of mean density profiles and fluctuation amplitudes in turbulent edge plasma. The simulations considered a neutral deuterium-electron plasma, evolving drift-fluid equations with a source term to compute initial steady-state turbulent density (for which a representative cross-sectional profile is shown in Figure 1R) and flow profiles for all regions in the domain, including within the limiter shadow. Using the same initial conditions, the simulation was then rerun, but with static ad hoc potentials (of order 50 V) applied to portions of the limiter surface to mimic the effect of local RF-rectified sheath potentials. Relative to the initial discharge, these imposed static potentials were shown to flatten the steady-state density profile, enable deeper penetration of density fluctuations within the antenna aperture, and increase the transport of impurity species through convective cell formation. These results strongly support the hypothesis that RF sheath potentials may strongly influence edge plasma turbulence and transport evolution.

In this work, we explore a related but somewhat opposite question – how do edge plasma turbulence and transport profiles influence the formation of RF sheaths? The timescale disparity between characteristic RF wave effects (of order tenths of microseconds for convergence to steady-state) and transport timescales (of order tenths of milliseconds) makes fully self-consistent simulation of these effects numerically challenging. Nevertheless, this disparity provides reasonable justification for treating these turbulent density profiles as constant in time in our initial simulations of RF and sheath effects, so we begin by examining RF wave excitation, propagation, and sheath formation in such static profiles. For this modeling, we use the VSim (Vorpal) code [7], a massively parallel, finite-difference time-domain code with a semi-implicit plasma wave solver [8]. VSim also exercises a newly implemented nonlinear sheath model [9] which parametrically computes RF sheath potential amplitudes and sheath widths from local plasma and surface conditions.

To run VSim, static steady-state turbulent density profiles generated by Hermes are interpolated onto the finer VSim grid, and the flux-tube geometry (limiters, end plates, etc.) is likewise reproduced on this grid. Antenna straps (not present in the Hermes runs) are also added; these are radially positioned just inside the aperture and extend from x=0.52 m to x=0.68 m, and from z=0.33 m to 0.67 m. In single-strap configuration (shown in Figure 1L), the strap runs from y=7.37 m to y=7.58 m; in double-strap configuration, the middle (vertical) third of the single strap is removed so that the remaining portions extend from y=7.37 m to 7.44 m (bottom strap) and y=7.51 m to 7.58 m (top strap). RF current is driven in the strap(s) at 60 MHz at various fixed amplitudes attained after an initial rampup period (see Figure 2). For simplicity, power feeds to the antenna straps are not included in the model; rather, we impose periodic current density sources within the 3D strap region shown in Figure 1L. For two-strap configurations, the straps may be driven with either 0-0 or 0-π phasing.

RF sheath boundary conditions [9] are imposed on all shaded surfaces (limiter, antenna, and wall) shown in Figure 1L. Periodic boundary conditions are used in the z-direction. An absorbing layer imposed at the lower-x face of the computational domain captures and damps outgoing RF waves without reflection. The simulations use a uniform 3D Cartesian grid with grid spacing 1.5 mm. Computational resource requirements for the VSim simulations can be reduced by truncating the flux-tube domain in the parallel (y) direction. For the simulations presented here, a parallel domain of length 3.0 m centered on the antenna was used; sheath formation on limiter surfaces appears to be relatively insensitive to the parallel domain length.

The amplitude of the current in the RF antenna straps was initially chosen such that in the single-strap case, the Poynting flux exiting the antenna aperture (in the -x direction, in Figure 1L) had a value of 1 MW/m^2. For two-strap cases, the same current density was used to drive the antenna straps, though since the physical volume of the individual straps is reduced the Poynting flux is also decreased, as shown in Figure 2. The observed variation of the outgoing Poynting flux with strap phasing (0-0 or 0-π) also aligns reasonably with expectations.

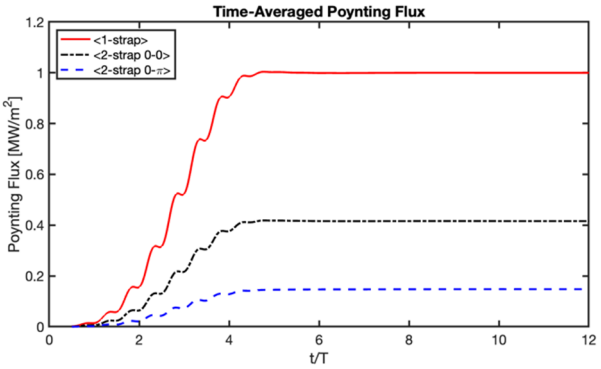

Fig. 2. Time-averaged Poynting flux exiting the antenna aperture for various antenna configurations (single-strap, double-strap with 0-0 phasing, double-strap with 0-π phasing).

A number of interesting physical effects are observed in these simulations.

Observed RF-rectified sheath potential amplitudes strongly correlate with the plasma density on the high-density (S<0) side of the S=0 resonant surface. RF-rectified steady-state sheath potentials observed on inner limiter surfaces (i.e., the antenna-facing x-z surfaces of Figure 1L) peak in large-amplitude, localized hotspots that correlate with higher values of the plasma density. In Figure 3, both local densities and RF sheath potentials are shown at the upper inside limiter face for the single-strap antenna configuration after the sheath potential has come to steady state. The high sheath potentials observed are likely a consequence of the single-strap monopole antenna configuration. Unexpectedly, the locations of highest sheath potential occur above the lower hybrid resonant surface (S=0), in regions where S<0. Recent experimental results on low-density WEST discharges, reported in these proceedings [10], suggest that sheath potential amplitude should decrease with increasing density in the S<0 regime. The cause of this discrepancy is not well-understood; the proximity of the hotspots to the S=0 transition region (see Fig. 1, wherein this region closely tracks the limiter edge) may play a role.

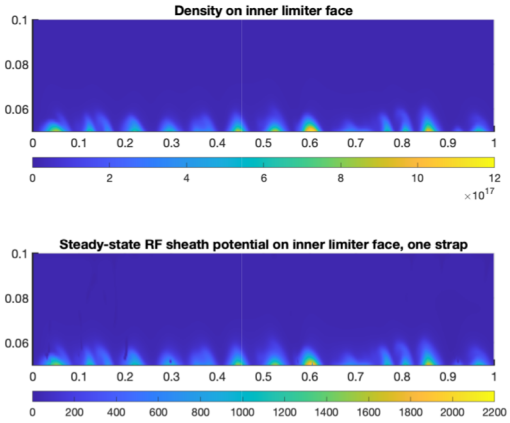

Fig. 3. (Top) Plasma density (as modeled by Hermes) on the antenna-facing surface of the top limiter plate. (Bottom) Steady-state RF-rectified sheath potential amplitudes observed at this surface as RF waves propagate through the Hermes density profile.

Wave power appears to flow along density filaments. Consistent with the theory proposed at the previous RF-Topical conference by Tierens *et al*. [11], and corroborating experiments presented at this conference by Larson [12], we are exploring whether these high sheath potentials arise in connection with surface waves, which may be excited and propagate in the parallel direction along high-density filaments bordering the antenna aperture. Analytic 1D dispersion calculations indicate that undamped parallel propagation along density filaments near the front of the aperture is indeed possible, though the anticipated parallel wavelength significantly exceeds the aperture size. Poynting flux measurements in the parallel and antiparallel directions, which reach values that are nearly 20% of those observed to exit the aperture toward the plasma core, are consistent with the hypothesis.

Hotspots are persistent even when RF power is reduced. Scatter plots of the density and sheath potential at the limiter surface (i.e. plotting the dependent variables of Figs. 3T and 3B against one another) clearly demonstrate the linear correlation between these variables at high density, as shown in the top panel of Fig. 4. As the strap current amplitude is lessened, so as to reduce the outgoing RF power tenfold or one-hundredfold, an increasing number of points on the limiter surface diverge from this linear correlation between sheath potential and density. Nevertheless, the trend is still apparent even at considerably reduced RF power. Unexpectedly, at these low powers a few high-

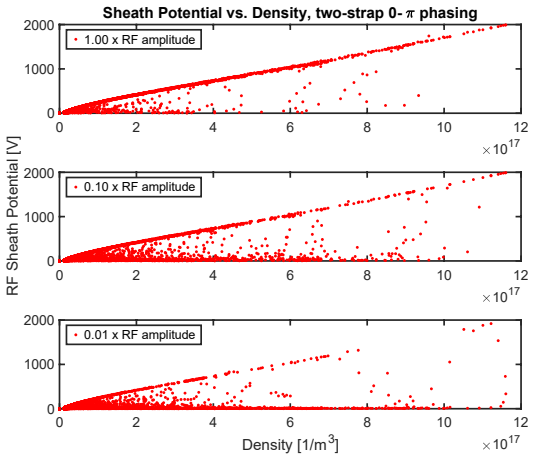

Fig. 4. Correlation of plasma density and RF-rectified steady-state sheath potential at all points on the top inner limiter surface, for a double-strap antenna run with 0-π phasing. For the baseline scenario (top), strong linear correlation is observed; hotspots (akin to those shown in Fig. 3) arise at points with both high sheath potential and high density. Even as power is reduced tenfold (middle) or one-hundredfold (bottom), this linear trend persists, and a few hotspots of comparably high amplitude can still be observed. The S = 0 resonant surface occurs at $n_0 = 1.75 \times 10^{17}$ / m^3.

density, high-amplitude hotspots still persist; we have not yet determined whether these unexpected hotspots are numerical artifacts or whether they have some physical basis. In any case, the observed density/potential correlation is broadly consistent with previous simulations carried out by Migliore *et al*. [13], which explored the reduction of near-field RF sheath

potentials in response to various antenna configurations (varied strap phasing, antenna power, etc.) aiming to minimize RF-induced image currents.

Regions of high $E_{||}$ near the limiter face are not strongly correlated with plasma density. Plots of the local parallel electric field adjacent to the limiter surface (as shown in Fig. 5 for a two-strap antenna with 0-π phasing) bear little resemblance to the plots in Fig. 3.

It is interesting to consider that the parallel species currents, which in the bulk (presumptively cold) edge plasma satisfy

$$\partial J_{||s}/\partial t = \omega_{ps}^2 E_{||} \quad (1)$$

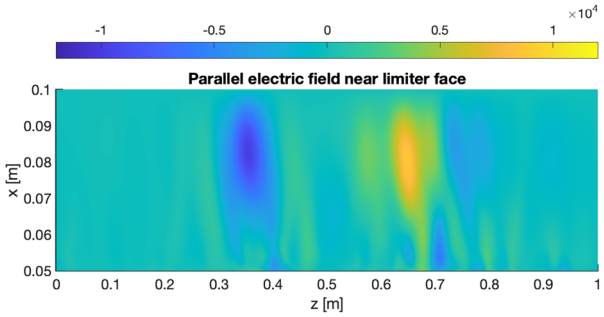

Fig. 5. The parallel electric field on the antenna-facing surface of the top limiter plate, as predicted by the VSim simulations, has minimal correlation with the local plasma density or sheath potential.

arise from the product of this parallel electric field with the plasma density (as contained within the square of the species plasma frequency ω_{ps}). Parallel currents entering the RF sheath should vary linearly with both quantities.

The flux-tube model qualitatively reproduces RF/material-interaction physics observed in more complex simulations of fusion-relevant experiments. The VSim code has been used previously by members of this research team to predictively model plasma-material interaction in SPARC [14], attempting to quantify the degree to which the operation of ICRF antennas will enhance the baseline thermal impurity sputtering expected in the reactor. Although the SPARC antenna geometry is considerably more sophisticated than the flux-tube simulations we have carried out in this work (see Fig. 6), and the L-mode-adjacent density profiles used in the SPARC simulations likewise differ considerably from the turbulent profiles predicted by Hermes, there are a number of important qualitative similarities. In both scenarios, significant interplay between density, antenna geometry, and RF sheath formation is present in the far scrape-off layer. While the primary objective of ICRF antenna operation is to launch fast waves that propagate radially inward from the antenna straps to reach the plasma core, conditions in the far-SOL may also permit the propagation of parallel slow/surface waves along local magnetic field lines/density filaments. Such conditions typically occur in spatial gaps much smaller than the expected parallel wavelength (e.g., between an antenna strap and a limiter or Faraday shield), but may nevertheless give rise to locally high regions of RF-rectified sheath

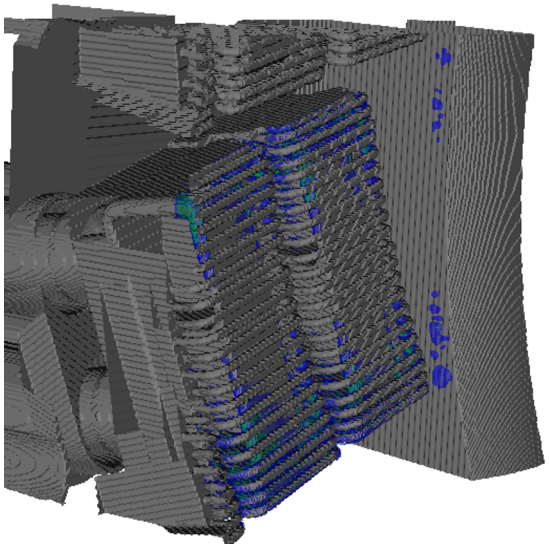

Fig. 6. Cutaway portion of the SPARC ICRF antenna, showing two antenna straps (positioned vertically behind the near-horizontal Faraday shields). Sheath potential hotspots of order 100 V, as modeled by VSim, appear on the adjacent limiter surface.

potential as power propagates along field lines and strikes a material surface. Despite the flux-tube model's new coordinate system (Cartesian rather than toroidal) and its simpler antenna and limiter geometry, these salient features of the SPARC discharges are well-reproduced by the model at considerably reduced computational cost (see Fig. 7).

Future research efforts that exercise this model will focus on quantifying the parallel propagation of RF power along density filaments, and its relationship with the RF-rectified sheath potentials that form on material surfaces intercepted by such filaments. We also plan to examine correlations between observed sheath potentials at top and bottom limiter points connected by magnetic field lines, and to implement in VSim more general RF sheath models which take into account the physics of DC parallel current flow. In Hermes simulations, the use of imposed limiter potentials which linearly correlate with the local plasma density, and the effect of these (arguably more self-consistent) potentials on edge plasma turbulence and transport, is also of interest. The development of a more physically self-consistent coupling workflow between Hermes and VSim is a related long-term objective. Lastly, we are hopeful that the physical insights afforded by the relatively simple flux-tube model presented here can facilitate better understanding of the complex interplay between RF waves, sheaths, and material interactions in the plasma edge.

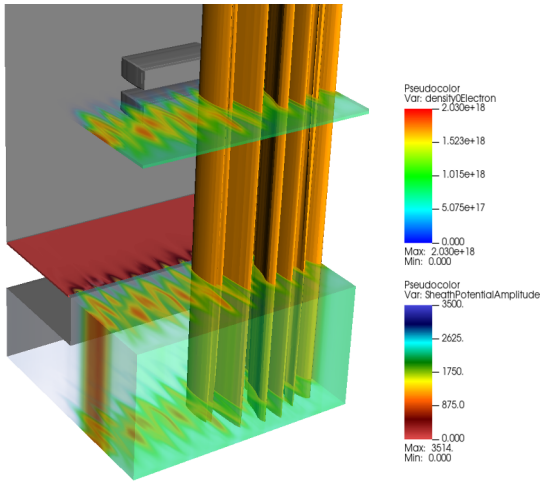

Fig. 7. 3D rendering of the correlation between local plasma density and RF-rectified sheath potential on the limiter face, as predicted by the flux-tube model implemented in VSim and Hermes. It is hoped that the reduced computational cost and the relative simplicity of this model (relative to 3D models which incorporate realistic density profiles and antenna hardware) will more easily enable greater understanding of RF-plasma-material interactions in the plasma edge.

This work was financially supported by the U.S. Department of Energy, Office of Science, Office of Advanced Scientific Computing Research and Office of Fusion Energy Sciences, Scientific Discovery through Advanced Computing (SciDAC) program under Award Number DE-SC0024369, the SciDAC Center for Advanced Simulation of RF - Plasma - Material Interactions (PIs P. T. Bonoli and N. Bertelli). This research used resources of the National Energy Research Scientific Computing Center, a DOE Office of Science User Facility supported by the Office of Science of the U.S. Department of Energy under Contract No. DE-AC02-05CH11231 using NERSC award FES-ERCAP0031364.

References

1. D.A. D'Ippolito et al., Analysis of RF sheath interactions in TFTR, Nucl. Fusion **38**, 1543 (1998). https://doi.org/10.1088/0029-5515/38/10/311
2. W. Zhang et al., Scattering of Ion Cyclotron Range of Frequency waves by filaments and ELMs, Nucl. Fusion **60**, 096001 (2020). https://doi.org/10.1088/1741-4326/ab9a0b
3. W. Zhang et al., Interaction between filaments and ICRF in the plasma edge, Nucl. Mater. Energy **26**, 100941 (2021). https://doi.org/10.1016/j.nme.2021.100941
4. M. V. Umansky, B. D. Dudson, T. G. Jenkins, J. R. Myra, and D. N. Smithe, Modeling of convective cells, turbulence, and transport induced by a radio-frequency antenna in the tokamak boundary plasma, submitted to Plasma Phys. Control. Fusion, May 2025.
5. B. D. Dudson and J. Leddy, Hermes: global plasma edge fluid turbulence simulations, Plasma Phys. Control. Fusion **59**, 054010 (2017). https://doi.org/10.1088/1361-6587/aa63d2
6. B. Dudson, M. Kryjak, H. Muhammed, P. Hill, and J. Omotani, Hermes-3: Multi-component plasma simulations with BOUT++, Comput. Phys. Commun. **296**, 108991 (2024). https://doi.org/10.1016/j.cpc.2023.108991
7. C. Nieter and J. R. Cary, VORPAL: a versatile plasma simulation code, J. Comp. Phys. **196**, 448 (2004). https://doi.org/10.1016/j.jcp.2003.11.004
8. D. N. Smithe, Finite-difference time-domain simulation of fusion plasmas at radio-frequency timescales, Phys. Plasmas **14**, 056104 (2007). https://doi.org/10.1063/1.2710784
9. J. R. Myra, Physics-based parametrization of the surface impedance for radio-frequency sheaths, Phys. Plasmas **24**, 072507 (2017). https://doi.org/10.1063/1.4990373
10. R. Diab et al., Direct Measurement of ICRF-Enhanced Plasma Potentials on WEST Using Reciprocating Emissive Probes, 25th Topical Conference on Radio-Frequency Power in Plasmas, 19-22 May, Hohenkammer, Germany.
11. W. Tierens, R. Bilato, N. Bertelli, S. Shiraiwa, J. Myra, and L. Colas, Filaments as the origin of HHFW losses in NSTX, AIP Conf. Proc. **2984**, 030006 (2023). https://doi.org/10.1063/5.0162406
12. J. Larson, B. Van Compernolle, R. Pinsker, T. Carter, and W. Tierens, Wave-filament Interaction Experiments on the LArge Plasma Device (LAPD), 25th Topical Conference on Radio-Frequency Power in Plasmas, 19-22 May, Hohenkammer, Germany. https://www.ipp.mpg.de/5533973
13. C. Migliore, J. C. Wright, M. Stowell, and P. T. Bonoli, Using the Stix finite element RF code to investigate operation optimization of the ICRF antenna on Alcator C-Mod, Nucl. Fusion **63**, 106006 (2023). https://doi.org/10.1088/1741-4326/acee11
14. T. G. Jenkins, D. N. Smithe, A. Yue, D. Curreli, M. Rezazadeh, M. W. Brookman, and M. L. Garrett, Time-domain modeling of RF sheath potentials for impurity production estimates in SPARC, APS Division of Plasma Physics, Denver, Colorado, USA, October 30 - November 3 (2023).